Reducing Deck Cracking in Composite Bridges by Controlling Long Term Properties

Fatmir Menkulasi, Doug Nelson, Carin L. Roberts Wollmann and Tommy Cousins

Synopsis: Composite concrete bridges are widely used because they combine the advantages of precast concrete with those of cast-in-place concrete. However, because of the difference in shrinkage properties between the girder and the deck and because of the sequence of construction, the deck is subject to differential shrinkage tensile stresses. These tensile stresses may lead to excessive cracking. This paper demonstrates how the likelihood of deck cracking due to differential shrinkage can be reduced and how consequently the resistance of composite concrete bridges against time dependent effects can be enhanced by choosing a deck mix with low shrinkage and high creep. An experimental study on the long term properties of seven deck mixes is presented to identify a deck mix with the aforementioned properties. A comparison of three composite concrete bridge systems used for short-to-medium-span bridges is performed to identify the bridge system that is most resistant against time dependent effects. The mix with saturated lightweight fine aggregates appears to best alleviate tensile stresses due to differential shrinkage and the bridge system with precast inverted T-beams and tapered webs appears to be the most resistant.

Keywords: composite bridges, cracking, creep, differential shrinkage, tensile stresses

ACI member **Fatmir Menkulasi** is an assistant professor in the College of Engineering and Science at Louisiana Tech, Ruston, LA. He is an associate member of ACI Committees 343 and 423. His research interests include the development of resilient and sustainable composite bridge systems. He is a licensed Professional Engineer in Virginia, USA.

ACI member **Doug Nelson** is a structural engineer with Figg Engineering in Dallas, TX. His research interests include the application of cementitious composites to increase the durability and longevity of bridges.

Carin L. Roberts Wollmann, FACI, is a Professor in the Via Department of Civil and Environmental Engineering at Virginia Tech, Blacksburg, VA. She is chair of ACI committee 423, and member of 239 and 318B. Her research interests include reinforced and prestressed concrete structures and bridge design and construction. She is a licensed Professional Engineer in North Carolina, USA.

ACI Member **Tommy Cousins** is a Professor in the Glenn Department of Civil Engineering, Clemson University, Clemson, SC. He is a member of ACI Committee 408 and associate member of 440. His research interests include long term bridge monitoring, behavior of bridge structures and use of high performance materials. He is a licensed Professional Engineer in Louisiana, USA.

INTRODUCTION

State departments of transportation expend significant effort and resources on the construction of durable bridges. A durable bridge is defined as one with a long service life and low maintenance requirements, which lead directly to low life-cycle costs. Deterioration of concrete bridges is the result of harmful environmental conditions such as: water, deicing chemicals, freezing temperatures, mechanical abrasion etc. The most serious threats to durability are generally posed by combinations of two or more of these conditions [1]. Cracks in concrete bridge decks provide easy access for water and deicing chemicals, which shorten the life of the deck, especially in bridges subject to aggressive environments. Both materials increase the effects of freeze-thaw damage, while the deicing chemicals lead to higher concentrations of chlorides, and subsequently, corrosion of reinforcing steel [2]. While there is no general consensus on the influence of crack width on corrosion of reinforcing steel, there is agreement that thickness and porosity of concrete covering the reinforcement are important parameters influencing corrosion [3]. There are generally two approaches that can be taken with regards to cracking.

The first approach is to design concrete members not to crack under service loads. To do this the sources of cracking must be identified and measures taken to reduce the potential for the development of cracks. These measures include designing not only for the mechanical loads but also for the structural effects of restrained deformations. Examples of restrained deformations include differential settlements, differential shrinkage, temperature gradients, and uniform changes in temperature. Measures that can be taken to reduce the potential for cracking include modifying concrete material properties and adjusting construction sequences and techniques. Article 3.3.2 of AASHTO [4] classifies force effects due to shrinkage and creep as permanent loads. In addition, Table 3.4.1-1 in AASHTO [4] stipulates the service and strength level load combinations which include the effects of shrinkage and creep. ACI 209.1R [5] provides guidance on the factors affecting drying shrinkage and creep and discusses the effect of mixture proportions, the environment and the effect of design and construction on shrinkage and creep. ACI 209.2R [6] presents several models for calculating shrinkage strains and creep coefficients so that the structural effects of shrinkage and creep can be accounted for in the structural design.

The second approach is to design concrete members to crack under service loads and take measures to control crack width. For example code provisions provide guidelines on the amount of reinforcing steel needed to control crack width. A combination of both approaches is also a viable option, which includes taking measures to reduce the likelihood of cracking but also includes specifications for bar size, spacing and concrete cover to control crack width if cracks were to occur. The discussion presented in this paper focuses on cracking that may be developed in the cast-in-place deck as a result of differential shrinkage and demonstrates how the likelihood of cracking in short-to-medium-span bridges can be reduced by controlling the long term properties of the deck concrete and by choosing a bridge system that is resistant against time dependent effects.

SCOPE OF STUDY

The scope of this study is to demonstrate the potential for differential concrete shrinkage to induce tensile stresses in cast-in-place bridge deck in excess of the tensile strength of concrete and recommend a deck mix that reduces the likelihood of cracking due to differential shrinkage. In addition, one traditional and two relatively new bridge systems intended for short-to-medium-span bridges are investigated for their resistance to tensile stresses resulting from time dependent effects. A series of seven deck mixes developed by the researchers at Virginia Center for Transportation Innovation and Research (VCTIR) are investigated by measuring: compressive strength, modulus of elasticity, splitting tensile strength, shrinkage, and creep. A numeric investigation and several finite element analyses are conducted with the purposes of simulating and quantifying the effects of differential shrinkage in short-to-medium-span bridges and ranking these three bridge systems in order of resistance to this phenomenon. The three bridge systems chosen for this investigation will be presented later in this paper.

RESEARCH SIGNIFICANCE

Excessive deck cracking leads to deck deterioration and expensive repair and rehabilitation procedures. Cracks in concrete bridge decks provide easy access for water and deicing chemicals to reinforcement, which shorten the life of the deck, especially in bridges subject to aggressive environments. One cause of excessive deck cracking is differential shrinkage between the cast-in-place concrete deck and the precast concrete girder. The restraint of the shrinkage of the deck by the girder creates tensile stresses in the deck which may exceed the tensile strength of deck concrete. This paper demonstrates how the likelihood of deck cracking in short-to-medium-span bridges can be reduced by controlling the long term properties of the deck and by choosing a bridge system that reduces the extent of critical tensile stresses in the deck resulting from differential shrinkage.

STRUCTURAL EFFECTS OF DIFFERENTIAL SHRINKAGE AND CREEP IN COMPOSITE SYSTEMS

The inherent difference in shrinkage and creep properties between a cast-in-place deck and precast girder will cause self-equilibrating stresses at the cross-sectional level in a composite system. Even if the composite girder is used in a single span simply supported bridge, these self-equilibrating stresses will form along the entire span of the bridge. The difference in shrinkage properties is exacerbated by the difference in age between the two components. As a result, when the cast-in-place deck is placed, it will tend to shrink while the majority of the shrinkage in the precast girder has already taken place. The restraint provided by the precast girder to the free shrinkage of the deck will create a tensile force in the deck while the free shrinkage of the deck will exert a compressive force in the precast girder. In addition, because the centroids of the precast and cast-in-place components are at different locations, this differential shrinkage will cause a positive curvature. The curvature will result in a prestress gain in the bottom layer of prestressing in the precast girder, whereas the compression force from the shrinkage of the deck will cause a prestress loss.

Figure 1 shows the redistribution of forces in a composite system consisting of a precast prestressed concrete girder and a cast-in-place deck. The time dependent strain at any fiber in the precast girder or cast-in-place deck can be calculated by summing the elastic and creep strains due to initial stresses, elastic and creep strains due to changes in stress, and the shrinkage strain (Eq. 1).

$$\varepsilon_t = \underbrace{\frac{\sigma_0}{E_0}\left(1+\varphi_{t,t_0}\right)}_{\textit{Term 1}} + \underbrace{\int_{t_0}^{t}\left[\frac{1}{E(\tau)}\frac{d\sigma(\tau)}{d\tau}\left(1+\varphi(t,\tau)\right)\right]d\tau}_{\textit{Term 2}} + \underbrace{\varepsilon_{sh,t}}_{\textit{Term 3}} \tag{1}$$

where

ε_t = total strain at time t

$\sigma_0, \sigma(\tau)$ = stress at time t_0 and τ, respectively

$E_0, E(\tau)$ = modulus of elasticity at times t_0 and τ, respectively

$\varphi_{t,t_0}, \varphi(t,\tau)$ = creep coefficient at time t due to load applied at time t_0 and τ, respectively

$\varepsilon_{sh,t}$ = shrinkage strain at time t

Term 1 represents the elastic and creep strains due to a stress applied at time t_0. Term 2 represents the elastic and creep strains due to changes in stress in the time interval t_0 to t. Term 3 represents the shrinkage strain at time t. Eq. 1 uses an integral type creep law for Term 2, which is a Volterra type integral, and uses the principle of

superposition of stepwise prescribed stress histories [7]. The integral term can be replaced by an algebraic expression if an aging coefficient μ is introduced [8,9]. Eq. 1 can then be reformulated as follows:

$$\varepsilon_t = \frac{\sigma_0}{E_0}\left(1+\varphi_{t,t_0}\right) + \frac{\Delta\sigma}{E_0}\left(1+\mu\varphi_{t,t_0}\right) + \varepsilon_{sh,t} \tag{2}$$

As defined earlier σ_0 represent initial stresses. These stresses can be created by forces and moments that are initially directly applied to the precast girder or the cast-in-place deck ($M_{Ddirect}^0$,$N_{Ddirect}^0$, $M_{Gdirect}^0$, $N_{Gdirect}^0$, $N_{psdirect}^0$) or by forces and moments that are initially applied to the composite system (M^0, N^0). For example an eccentric prestressing force in a pre-tensioned girder creates axial forces and bending moments that are applied directly to the girder in addition to the axial force applied directly to the prestressing strand. To utilize the free shrinkage and creep properties of the precast and cast-in-place concrete it is useful to decompose the internal forces and moment acting on the composite section, into forces and moments acting separately on the girder and deck (M_D^0,N_D^0, M_G^0, N_G^0, N_{ps}^0). Examples of axial forces and bending moment that are applied initially to the composite system include post-tensioning forces applied after the system is made composite and bending moments created due to superimposed dead loads.

The term Δσ in Eq. 2 represents the change in stress due to changes in axial forces and bending moments in the deck, girder or prestressing strands. These are denoted as ΔM_D, ΔN_D, ΔM_G, ΔN_G and ΔN_{ps} in Fig. 1. The changes in strains and stresses due to time dependent effects can be calculated by using equations of material constitutive relationships, equilibrium and compatibility. Menn [1] provides detailed guidance on how this analysis can be performed. Some of the theoretical background provided in Menn's book is presented below for convenience. For example the change in axial strain at the centroid of the deck and girder can be expressed by summing the creep strain due to initial axial forces, the elastic and creep strain due to the change in axial force over time and the free shrinkage strain (Eq. 3 and 5). The change in curvature in the deck and girder can be expressed by summing the creep curvature due to initial moments and the elastic and creep curvatures due to changes in these moments over time (Eq. 4 and 6). The change in prestressing strand strain over time can be simply calculated by dividing the change in stress in the strand by the modulus of elasticity of the strand (Eq. 7). The change is stress in the strand over time represents either a prestress loss or prestress gain due to differential shrinkage and creep.

In a statically determinate system, because there are no externally applied axial forces over time, the sum of changes in the axial forces in each component must equal zero (Eq. 8). In addition, in such a determinate system because there are no externally applied bending moments over time, the sum of moment about the centroid of the girder must equal zero (Eq. 9). Finally, assuming perfect bond between deck concrete, girder concrete and prestressing strands the axial strains at the centroid of each of these components can be inter-related by using the change in curvature and the distances between the centroids (Eq. 10 and 11). The assumptions made in this method of analysis are: a) plane sections remain plane, b) sections are un-cracked, c) creep and shrinkage properties are assumed to represent the average behavior of the whole cross-sections, or components thereof, in drying conditions, d) tensile creep is the same as compressive creep.

Equations 3 to 11 form a set of linear equations which can be solved simultaneously to determine the 9 unknowns caused by the time dependent effects $(\Delta\varepsilon_D,\ \Delta\varepsilon_G, \Delta\varepsilon_{ps}, \Delta X, \Delta N_D, \Delta N_G, \Delta N_{ps}, \Delta M_D, \Delta M_G)$. Initial and final stresses can then be calculated using Eq. 12-17. This method can be easily implemented in a mathematical analysis program, such as Mathcad 14 [10], or in a computer spreadsheet program. It should be noted that the approach used in Eq. 3-17 considers only stresses and strains in one direction at a time. Finite element analysis can be used to account for the 3D state of stress and quantify time dependent effects when such an option is available. Both of these methods are used in this paper to determine the structural effects of differential shrinkage and shrinkage induced creep. Because differential shrinkage can cause tensile stresses in the deck that may exceed the tensile strength of concrete, a deck mix with low shrinkage will reduce the likelihood of cracking. In addition, a deck mix with high creep will alleviate the tensile stresses created as a result of differential shrinkage. The following section presents an experimental investigation on seven deck mixes with the purpose of identifying the mix with lowest free shrinkage and highest creep.

EXPERIMENTAL EVALUATION

Seven deck mixes developed by the researchers at VCTIR were put through a battery of tests to investigate their short term and long term properties. The deck mixes contained normal weight and light weight coarse and fine

aggregates. The mixture proportions for each mix design are provided in Table 1. The cementitious materials that were used were fly ash and blast furnace slag. To increase the workability of the mixes without increasing the water content, super plasticizer was used as needed. In addition, because bridge decks are structural components that are exposed to weather, an air-entrained mix is typically used to improve durability when the deck is subjected to freeze-thaw cycles and deicing salts. This improvement is typically accomplished by adding an air entraining agent. The resulting even distribution of pores in the concrete prevents large air voids from forming and breaks down the capillary pathways from the surface to the reinforcement [11]. Target material properties were as follows:

- Minimum compressive strength at 28 days = 4000 psi (28 MPa)
- Maximum coarse aggregate size for:
  - ✓ normal weight mixes = No.57 stone (1 in.) (25mm)
  - ✓ light weight mixes = ¾ in. (19 mm)
- Minimum cementitious materials content = 635 lbs/yd^3 (377 kg/m^3)
- Maximum water cementitious materials ratio for:
  - ✓ normal weight mixes = 0.45
  - ✓ light weight mixes = 0.43
- Slump = 4 in. to 7 in. (100 mm to 180 mm)
- Air Content = 6 ½ ± 1 ½ %

When a high-range water reducer (superplasticizer) was used, the upper limit on air content was increased by 1 %. One batch was placed for each concrete mix design.

Material Constitutive Relationships

$$\Delta\varepsilon_D = \frac{N^0_{Ddirect} + N^0_D}{E_D\,A_D}\,\varphi_D + \frac{\Delta N_D}{E_D\,A_D}\,(1+\mu\varphi_D) + \varepsilon_{SHD} \tag{3}$$

$$where: \qquad N^0_D = \frac{nA_D}{A_C}\,N^0 - \frac{M^0 a_D E_D A_D}{I_C E_G}$$

$$\Delta X = \frac{M^0_{Ddirect} + M^0_D}{E_D I_D}\,\varphi_D + \frac{\Delta M_D}{E_D\,I_D}\,(1+\mu\varphi_D) \tag{4}$$

$$where: \qquad M^0_D = \frac{M^0 E_D I_D}{E_G I_C}$$

$$\Delta\varepsilon_G = \frac{N^0_{Gdirect} + N^0_G}{E_G\,A_G}\,\varphi_G + \frac{\Delta N_G}{E_G\,A_G}\,(1+\mu\varphi_G) + \varepsilon_{SHG} \tag{5}$$

$$where: \quad N^0_{Gdirect} = -P_e + \frac{M^0 a_{ps} E_{ps} A_{ps}}{I_C E_G}\,, \qquad N^0_G = \frac{A_G}{A_C}\,N^0 + \frac{M^0 a_D E_D A_D}{I_C E_G}$$

$$\Delta X = \frac{M^0_{Gdirect} + M^0_G}{E_G I_G}\,\varphi_G + \frac{\Delta M_G}{E_G\,I_G}\,(1+\mu\varphi_G) \tag{6}$$

$$where: \qquad M^0_{Gdirect} = -P_e e + M_{Gself} + M_{Gslab}\,, \qquad M^0_G = \frac{M^0 I_G}{I_C}$$

$$\Delta\varepsilon_{ps} = \frac{\Delta N_{ps}}{E_{ps} A_{ps}} \tag{7}$$

Equilibrium

$$\Delta N_D + \Delta N_G + \Delta N_{ps} = 0 \tag{8}$$

$$\Delta M_G + \Delta M_D - \Delta N_D a + \Delta N_{ps} e = 0 \tag{9}$$

Compatibility

$$\Delta\varepsilon_D = \Delta\varepsilon_G - \Delta X\,(y_{Dbottom} - y_{Gbottom}) \tag{10}$$

$$\Delta\varepsilon_{ps} = \Delta\varepsilon_G + \Delta X\,(y_{Gbottom} - y_{psbottom}) \tag{11}$$

Stresses

$$\sigma_{D0} = \left(\frac{N^0_{Ddirect} + N^0_D}{A_D} + \frac{(M^0_{Ddirect} + M^0_D)}{I_D}\,y\right) \tag{12}$$

$$\sigma_{Dfinal} = \left(\frac{N^0_{Ddirect} + N^0_D + \Delta N_D}{A_D} + \frac{(M^0_{Ddirect} + M^0_D + \Delta M_D)}{I_D}\,y\right) \tag{13}$$

$$\sigma_{G0} = \left(\frac{N^0_{Gdirect} + N^0_G}{A_G} + \frac{M^0_{Gdirect} + M^0_G}{I_G}\,y\right) \tag{14}$$

$$\sigma_{Gfinal} = (\frac{N^0_{Gdirect} + N^0_G + \Delta N_G}{A_G} + \frac{(M^0_{Gdirect} + M^0_G + \Delta M_G)}{I_G} y) \quad (15)$$

$$\sigma_{psinitial} = (\frac{N^0_{psdirect} + N^0_{ps}}{A_{ps}}) \quad (16)$$

$$\sigma_{psfinal} = (\frac{N^0_{psdirect} + N^0_{ps} + \Delta N_{ps}}{A_{ps}}) \quad (17)$$

Short term properties

Short term properties determined for the deck mixes include compressive strength, splitting tensile strength, and modulus of elasticity. These short term properties are useful in assessing the quality of concrete and the response to short-term loads such as vehicle live loads [11]. Sometimes these short term properties are modified to account for the long term effects. For example, the Age Adjusted Effective Modulus (AAEM) method [8,9] accounts for the increase in strain due to creep of concrete under sustained loads by employing a reduced long term modulus of elasticity. The compressive strength, splitting tensile strength and modulus of elasticity were determined in accordance with ASTM C39 [12], ASTM C496 [13], ASTM C469 [14] respectively. The short term properties for all seven mixes are provided in Table 2, Table 3, and Table 4.

Experimental data for tensile strength and modulus of elasticity are compared to the values obtained using the equations in AASHTO [4]. These equations are provided in AASHTO [4] Section 5.4.2.4 and Section 5.4.2.6-7, respectively. When cracking is caused by the effects of flexure, AASHTO [4] provides a series of equations for the determination of modulus of rupture (f_r) for both normal-weight and light weight concrete. These values vary between $0.20\sqrt{f'c}$ to $0.24\sqrt{f'c}$ ($0.53\sqrt{f'c}$ to $0.64\sqrt{f'c}$) for normal weight concrete and between $0.17\sqrt{f'c}$ to $0.20\sqrt{f'c}$ ($0.45\sqrt{f'c}$ to $0.53\sqrt{f'c}$) for lightweight concrete, where f'_c is in ksi (MPa). The commentary of Section C5.4.2.6 states that data show that most modulus of rupture values are between $0.24\sqrt{f'c}$ and $0.37\sqrt{f'c}$ ($0.64\sqrt{f'c}$ and $0.98\sqrt{f'c}$). In addition, the commentary of Section C5.4.2.7 states that the given values may be un-conservative for tensile cracking caused by restrained shrinkage, anchor zone splitting, and other similar tensile forces caused by effects other than flexure and that the direct tensile strength stress (f_t) should be used in these cases. Equation 18 is taken from the commentary of Section 5.4.2.7 –Tensile Strength and may be used for normal weight concrete with specified compressive strengths up to 10 ksi (70 MPa).

Because the focus of this paper is potential cracking due to restrained differential shrinkage, Eq. 18 is used to compare calculated and tested tensile strength values. Equation 19 is used to calculate the tensile strength of mixes that contained light weight coarse aggregates and normal weight fine aggregates (sand-lightweight). There is no equation in AASHTO [4] that is applicable to the mixes that contained normal weight coarse aggregates and a mixture of normal weight and light weight fine aggregates. Because the normal weight aggregates represented the majority of aggregates in these mixes, Eq. 18 was used for comparison with tested values. However, as can be seen from the results in Table 3, Eq. 18 overestimated the tensile strength of the two mixes that contained a mixture of normal weight and lightweight aggregates. In the calculation of concrete tensile strength using Eq. 18 and 19, the tested values were used for the compression strength of concrete. Although in general, AASHTO's [4] equations overestimated the tensile strength of the investigated mixes, they provided reasonably good estimates for design purposes. The tensile strength of concrete is an important short term property because the likelihood of cracking is estimated by comparing the magnitude of tensile stresses created due to differential shrinkage with the tensile strength of the cast-in-place concrete deck. Table 3 provides also a summary of the tested tensile strength of the seven concrete mixes at 28 days. The mix with the lowest tensile strength was the one with normal weight coarse aggregates and saturated lightweight fines. The mix with the highest tensile strength was the mix with normal weight coarse aggregates and slag denoted (NWC-SL2). The mixes that contained lightweight aggregates exhibited lower tensile strengths at 28 days compared to the mixes that contained normal weight aggregates. However, the compressive strengths at 28 days of the lightweight mixes were not always lower than those of the normal weight mixes. For example, the mix with the highest compressive strength at 28 days was the mix with saturated lightweight coarse aggregates and slag (SLWC-SL), whereas the mix with the lowest compressive strength at 28 days was the mix with normal weight coarse aggregates and fly ash (NWC-FA).

$f_t = 0.23\sqrt{f'c}$ where f'_c is in ksi, or $f_t = 0.61\sqrt{f'c}$ where f'_c is in MPa (18)

$f_t = 0.20\sqrt{f'c}$ where f'_c is in ksi, or $f_t = 0.53\sqrt{f'c}$ where f'_c is in MPa (19)

$E_C = 33{,}000\ K_1 w_c^{1.5} \sqrt{f'c}$ where w_c is in k/ft^3 and f'c is in ksi (20)
$E_C = 1.76\ 10^{11}\ K_1 w_c^{1.5} \sqrt{f'c}$ where w_c is in kg/m^3 and f'_c is in MPa

Tested modulus of elasticity values for the seven mixes were compared with those calculated using Eq. 20 from AASHTO [4]. Tested unit weight and compressive strength values were used in the evaluation of Eq. 20. In general, Eq. 20 underestimated the modulus of elasticity of the seven investigated mixes, however, it provided reasonably fair estimates for design purposes. Modulus of elasticity is another short term property that plays an important role in the evaluation of composite bridge systems for the effects of differential shrinkage. Because in this study the quantification of stresses due to differential shrinkage is based on the age adjusted effective modulus method, a higher modulus of elasticity for the deck leads to higher tensile stresses in the deck. Conversely, a lower modulus of elasticity for the deck leads to a lower age adjusted effective modulus and represents a mix that can alleviate the tensile stresses in the deck created as a result of differential shrinkage. In addition, with time the modulus of elasticity of concrete increases, which is why the age adjusted effective modulus method employed in this study uses an aging coefficient, which accounts for this effect. Such an increase in the modulus of elasticity works against the concept of alleviating tensile stresses as a result of differential shrinkage because it makes the mix stiffer and less accommodating towards restrained deformations.

Table 4 provides a summary of the moduli of elasticity values for the seven mixes at 28 days. The mix with the lowest modulus of elasticity is the mix with saturated light weight coarse aggregates and fly ash. Whereas the mix with the highest modulus of elasticity is the one with normal weight coarse aggregates and slag denoted (NWC-SL2). The comparison of tensile strength and modulus of elasticity for the seven mixes illustrates how it is difficult to find a mix that embodies all the desired properties. For example the mix denoted NWC-SL2 had the highest tensile strength but also the highest modulus of elasticity.

Long term properties

Typically, compressive strength, tensile strength and modulus of elasticity of concrete increase with age, however, in this paper the phrase long term properties is used to describe shrinkage and creep properties of concrete. Shrinkage is considered to be a change in volume during hardening and drying under constant temperature, whereas creep is defined as increase in strain over time under constant stress. Shrinkage and creep tests were performed in accordance with ASTM C157 [15] and ASTM C512 [16], respectively. Creep specimens were loaded at 7 days and the applied load was maintained at approximately $0.4f'_{c_7}$ (where f'_{c_7} is the average cylinder compressive strength at 7 days). The time dependent properties of concrete are influenced by the environmental conditions at the time of placement and throughout its service life [11]. These properties are used in determining the structural effects of differential shrinkage and creep. ACI 209.2 [6] provides four models for calculating shrinkage and creep properties as a function of time. AASHTO [4] has its own models for creep and shrinkage. ACI 209.2 [6] states that: "The variability of shrinkage and creep test measurements prevents models from closely matching experimental data. The within-batch coefficient of variation for laboratory-measured shrinkage on a single mixture of concrete was approximately 8% [17]. Hence, it would be unrealistic to expect results from prediction models to be within plus or minus 20% of the test data for shrinkage. Even larger differences occur for creep predictions. For structures where shrinkage and creep are deemed critical, material testing should be undertaken and long-term behavior extrapolated from the resulting data." It should be noted that the tests performed on the deck mixes described in this investigation were performed only on one batch for each mix. It was outside the scope of study to investigate the repeatability and consistency of the results obtained from each mix. One of the purposes of this study was to demonstrate the structural effects of differential shrinkage and creep and how they may influence the durability of composite bridges. The next section describes the results from the shrinkage and creep tests and identifies the mix with the desired long term properties.

COMPARISON OF SHRINKAGE AND CREEP PROPERTIES FOR EACH MIX

Figure 2 shows the development of drying shrinkage strains with time for the seven mixes investigated. In this paper shortening strains are positive. Because the changes in shrinkage strains recorded after 70 days were generally negligible, shrinkage testing was stopped at 100 days. It is important to note that the measured shrinkage strains represent only drying shrinkage strains. Shrinkage specimens were moist cured for 7 days and were then exposed to drying. Table 5 provides a summary of the shrinkage strains at 100 days. The mix with the lowest shrinkage was the mix with normal weight coarse aggregates and saturated lightweight fine aggregates. The mix with the highest

shrinkage was the mix saturated light weight coarse aggregates and slag. Both mixes that contained saturated lightweight coarse aggregates exhibited the highest shrinkage strains.

Figure 3 shows the development of measured strains with time during the creep test. Figure 3(a) shows the total strain which is defined in Eq. 21. Total strain is equal to the summation of elastic strain, shrinkage strain and creep strain. Elastic strain is the strain measured immediately after the creep specimens are loaded. Shrinkage strain is the strain due to the shrinkage of the creep specimens during the creep tests and is measured from unloaded companion cylinders. Creep strain is the increase in strain in the creep specimens over time as a result of the applied load.

$$total\ strain = elastic\ strain + shrinkage\ strain + \ creep\ strain \tag{21}$$

Because the change in total strains recorded from the creep test after 80 days were negligible, creep tests were terminated at a 106 days. Figure 3(b) shows the shrinkage strain measured in the creep specimens, which was deducted from the total strain to obtain the stress induced strain. Figure 3(c) shows the stress induced strain which is defined in Eq. 22. Stress induced strain is the strain caused only by the sustained load (or sustained stress) over time and can be expressed as the summation of the elastic strain and creep strain. Alternatively, stress induced strain can be expressed as the total strain measured in the creep specimens minus the shrinkage strain measured in unloaded companion cylinders.

$$stress\ induced\ strain = elastic\ strain + \ creep\ strain \qquad or \qquad stress\ induced\ strain = Total\ strain - shrinkage\ strain \tag{22}$$

Figure 3(d) shows the creep strain. Creep strain was obtained from deducting the elastic strain from the stress induced strain. One of the parameters used in the analysis for time dependent effects is the creep coefficient. Creep coefficient is the ratio of creep strain to the initial elastic strain (Eq. 23).

$$creep\ coefficient = \frac{drying\ creep\ strain}{initial\ elastic\ strain} \tag{23}$$

Table 6 provides a summary of the experimental data from creep tests. Elastic strains for the two mixes containing saturated lightweight coarse aggregates are higher than the rest of the mixes. This is expected because lightweight mixes typically have lower moduli of elasticity compared to normal weight mixes (as shown in Table 4). Although there were several differences between the shrinkage strains measured during the shrinkage tests and those measured from the unloaded companion cylinders during the creep tests, there were also some similarities. For example the NWC-SLWF, NWC-SL2 and NWC-SLWC-SL mixes exhibited the lowest shrinkage strains during both, shrinkage and creep tests. The lowest shrinkage strain however in the creep tests was measured in the NWC-SL2 mixes as opposed to the NWC-SLFW mix. Shrinkage strains measured during the creep test in the NWC-FA, NWC-SL1, SLWC-FA and SLWC-SL were also not entirely consistent with those measured from the shrinkage prisms. The highest disparity was observed in the shrinkage measurements for the SLWC-SL mix. During the creep tests this mix exhibited the lowest shrinkage strain compared to NWC-FA, NWC-SL1 and SLWC-FA mixes, whereas the data from the shrinkage prisms revealed the opposite. Despite these differences, the lowest average shrinkage strain from shrinkage and creep tests was still exhibited by the NWC-SLWF mix, which was identified as the mix with the lowest drying shrinkage strain during the shrinkage tests. Additionally, the shrinkage strains obtained from both tests agree well for the NWC-SLWF mix.

Because creep strain is calculated by subtracting elastic and shrinkage strains from the total strain the magnitude of the elastic and shrinkage strains plays an important role in this determination. In this study creep coefficient is used as the metric for comparing creep properties of the seven mixes, because it is this coefficient that is employed in the age adjusted effective modulus method.

Table 7 provides a summary of the long terms properties of the seven investigated mixes. The NWC-SLWF mix exhibited the lowest shrinkage, whereas the SLWC-SL mix exhibited the highest one. The NWC-SLWF mix also exhibited the highest creep coefficient, whereas the SLWC-SL mix exhibited the lowest creep coefficient. While it may be typically difficult to find a mix that exhibits both low shrinkage and high creep properties, in this study the NWC-SLWF mix possessed both of these characteristics and is considered to be the most desirable mix, whereas the

SLWC-SL mix is considered to be the least desirable one. For other situations where the combination of low shrinkage and high creep may not be possible, priority should be given to a mix with the lowest shrinkage because it is the free shrinkage of the deck that serves as a catalyst for the creation of tensile stresses in the cast-in-place topping and potentially excessive cracking. In addition, sensitivity studies can be performed for a given structure to determine the influence of the short and long term properties of the concrete materials on the structural effects of shrinkage and creep.

NUMERIC EXAMPLE

To illustrate the advantages of a deck mix with low shrinkage and high creep a composite bridge system with adjacent voided slabs is considered. This type of system is typically used for short-to-medium-span bridges. Because the adjacent precast voided slabs serve as stay-in-place formwork, this system offers accelerated bridge construction and replacement by eliminating the need for site installed formwork. Figure 5 shows a typical transverse cross-section for this bridge system. The cross-sectional dimensions shown in Fig. 5 represent those used in a two-span continuous bridge constructed during the spring of 2014 near Richmond, VA. Prestressing and mild steel reinforcing details are not shown for clarity. Each span is 41.5 ft (12.7 m). A time dependent analysis using the age adjusted effective modulus method and Menn's [1] approach described earlier in this paper was conducted with the purpose of quantifying the distribution of initial and final stresses in such a composite bridge system. A total of seven analyses were conducted with the purpose of exploring the influence of the long term properties of the seven deck mixes on the final distribution of stresses in this composite bridge system. The variables in each analysis consisted of the tested short and long term properties of each deck mix. Because the contract documents specified an age of 90 days for establishing continuity, the ultimate shrinkage strain and the ultimate creep coefficient for the precast voided slab were taken equal to zero. The age of continuity refers to the time when the cast-in-place deck is placed over the adjacent precast voided slabs, making the two-span bridge continuous. This time starts after the fabrication of the individual precast voided slabs. 90 days is considered a long enough time to allow the majority of the shrinkage and creep to take place in the precast voided slab. The aging coefficient was taken equal to 0.7. This investigation was also conducted with the purpose of revealing which investigated deck mix offers the best combination of short term and long term properties with regards to minimizing the tensile stresses in the deck as a result of differential shrinkage.

Figure 6(a) shows the distribution of the initial longitudinal normal stresses in the precast voided slab due to its self-weight, the prestressing force and the weight of the cast-in-place topping. Because the adjacent precast voided slabs serve as stay-in-place formwork for the cast-in-place topping, they support the wet weight of the topping and initial stresses in the topping are zero. In addition, the differences in the initial stress distribution along the depth of the girder among the deck mixes is because of the different units weights of each topping mix. With time, the composite section will be subject to additional stresses due to differential shrinkage as the cast-in-place topping will try to shrink and the precast girder will tend to restrain this shrinkage. These additional stresses due to time dependent effects are illustrated in Fig. 6(b). The combination of the initial stresses and those created due to time dependent effects is shown in Fig. 6(c), which highlights the variation of final stresses depending on which topping mix is selected. For example if the NWC-SLWF mix is selected, the maximum final tensile stress at the bottom of the cast-in-place topping is 0.214 ksi (1.5 MPa). Whereas, if the SLWC-SL mix is selected then the maximum tensile stress at the bottom of the cast-in-place topping can be as high as 0.756 ksi (5.2 MPa), which is greater than the modulus of rupture for the corresponding mix. Table 8 provides a summary of the maximum tensile stresses created at the bottom of cast-in-place topping for each of the investigated mixes. It also provides a comparison between the maximum tensile stress at the bottom of the deck and the corresponding tensile strength of the mix used in that analysis. As can be seen, the lowest ratio is provided by the mix that has normal weight coarse aggregates and saturated lightweight fine aggregates, whereas the highest ratio is provided by the mix that contains saturated lightweight coarse aggregates and slag. Only two of the mixes provided ratios that were smaller than one, which means that if the other mixes are used for the cast-in-place topping then the bridge may exhibit transverse cracks along both spans. It should be noted that in the time dependent analysis presented herein, the short and long term properties were based on the tested values for each mix and ultimate shrinkage strains and creep coefficient were not adjusted to account for the relative humidity at the bridge site and the volume to surface ratio of the structural components. The purpose of this analysis is to demonstrate how the long term properties of the deck mix can influence the resistance of the composite bridge system against time dependent effects. As a result, it is essential to specify a topping mix with low shrinkage and high creep to reduce the likelihood of excessive cracking and consequently increase the longevity of composite concrete bridges.

FINITE ELEMENT ANALYSES

The method illustrated in Eq. 3-17 using the age adjusted effective modulus is a sectional analysis method and can provide the distribution of longitudinal and transverse normal stresses due to time dependent effects for any given composite cross-section. Along the longitudinal axis of the bridge the voided slab composite section is prismatic and the results of time dependent analysis based on Eq. 3 to 17 will apply at any given transverse cross-section. However, because of the presence of the voids, the voided slab system is not prismatic in the transverse direction and the results of the time dependent analysis performed on a section by section basis will vary. To account for the interaction of these adjacent longitudinal sections a finite element model representing a typical transverse composite cross-section of the voided slab system was created. The material properties for the deck mix with normal weight coarse aggregates and saturated light weight fines were selected for this investigation because this mix had the best long term properties. To simulate the effects of differential shrinkage, the cast-in-place topping was subjected to a uniform decrease in temperature. The magnitude of the decrease in temperature was chosen such that when multiplied with the coefficient of thermal expansion for concrete resulted in a strain equal to the tested shrinkage strain at 100 days for the selected deck mix (Eq. 24). No temperature effect was applied to the girder, to be consistent with the earlier assumption that when continuity is established the majority of the shrinkage and creep in the girder have already taken place. Creep effects were simulated using an age adjusted effective modulus (Eq. 25). Poisson's ratio for both mixes was taken as 0.2. The finite element model for the typical composite voided slab cross-section was for a simply supported beam with the purpose of investigating only the effects of differential shrinkage at a cross-sectional level and not those due to restraint moments that are present in a multi-span bridge application. The length of the span was 41.5 ft (12.7 m). A 2 in. (51 mm) mesh was used for both the cast-in-place topping and the precast voided slab.

$$\Delta T_{deck} = \frac{\varepsilon_{deck\ at\ 100\ days}}{\alpha_{concrete}} \tag{24}$$

where:
$\varepsilon_{deck\ at\ 100\ days}$ = shrinkage strain at 100 days for NWC-SLWF deck mix (215 ue)
$\alpha_{concrete}$ = coefficient of thermal expansion for concrete (6.5 x 10^{-6} / ºF)
ΔT_{deck}= uniform decrease in temperature to simulate the effects of differential shrinkage (33 ºF)

$$E_{AAEM} = \frac{E_{deck}}{\left(1 + \mu\varphi_{deck\ at\ 100\ days}\right)} \tag{25}$$

where:
E_{AAEM} = age adjusted effective modulus for NWC-SLWF deck mix to account for creep effects
E_{deck} = modulus of elasticity for NWC-SLWF deck mix
μ = aging coefficient (taken as 0.7)
φ_{deck} = creep coefficient at 100 days for NWC-SLWF deck mix

Figure 7(a) shows a comparison of the magnitude and distribution of longitudinal normal stresses caused by differential shrinkage obtained based on Eq. 3 to 17 with those obtained from the finite element model. The longitudinal stresses in the finite element model were obtained at mid-width of the composite cross-section. There are some small differences in the magnitude of these stresses, because the values obtained from Eq. 3 to 17 are based on a sectional analysis using a one-dimensional stress state and represent the average behavior of the typical composite cross-section. Whereas those obtained from the finite element model account for the interaction between sections above the voids with those above the precast webs and also account for the three-dimensional stress-state. The results obtained from Eq. 3-17 provide a reasonable estimation of the stresses due to time dependent effects for design purposes and are a viable alternative to finite element analysis. Figure 7(b) illustrates that the location where the tensile stresses in the cast-in-place topping are highest is the interface between the girder and the deck. In addition, because the model represents a simply supported beam application, the magnitude of these stresses is relatively uniform along the span of the beam. Accordingly, if the highest tensile stress in the cast-in-place topping exceeds its tensile strength, transverse cracks will likely develop along the entire span of the beam. The spacing of these cracks will depend on the bond strength between the reinforcing steel and the surrounding concrete.

To compare the relative resistance of the voided slab system (Fig. 8(a)) against time dependent effects two other bridge systems were investigated. The second one is shown in Fig. 8(b) and consists of adjacent precast Inverted T-beams with straight webs and a cast-in-place topping. This bridge system was identified in 2004 in France during a

scanning tour funded by FWHA and AASHTO and has been used on several bridges in the state of Minnesota. The third system is similar to the second one with the exception that the precast webs are tapered rather than straight (Fig. 8(c)). This bridge system was implemented for the first time in Virginia for the replacement of a two-span continuous bridge on US 360 near Richmond, VA. The overall depth of the composite cross-section in the two inverted T-beam models was the same with the voided slab composite system. The width of the precast inverted T-beams was 6 ft (1.8 m). The width of the flange was 12 in. (300 mm), whereas the thickness of the flange was 4 in. (100 mm). The angle for the tapered webs in the system implemented in Virginia was 45°. The thickness of thinnest portion of the topping in both inverted T-beam systems matched that used in the voided slab system and was 7.5 in. (190 mm). The investigation of differential shrinkage induced stresses in the longitudinal and transverse directions of the bridge was of interest to explore the likelihood of transverse and longitudinal cracking, respectively.

Figure 8 shows transverse and longitudinal normal stress contours caused by differential shrinkage and shrinkage induced creep. In the voided slab system, longitudinal tensile stresses are highest at the precast-CIP interface (Fig. 8 (a)), which is consistent with the results presented in Fig. 6 and Fig. 7. Similarly, transverse tensile stresses are also highest at the interface between the precast and cast-in-place components. The same applies for the inverted T-beam systems, except that in these systems the interfaces between the precast and cast-in-place components are at two different elevations, with the interface between the top of the precast web and cast-in-pace topping being the most critical. Hence, reducing the length of this interface will help reduce the extent of potential cracking due to time dependent effects. Tensile stresses also develop in the cast-in-place topping at the interface between the precast flange and cast-in-place topping, however these stresses reduce towards the top of the composite cross-section and are compressive in the upper portions of the cast-in-place topping. Because it is the top of the cast-in-place topping that is subject to water and deicing salts these locations are not critical compared to the portion of the topping above the precast web where the entire cast-in-place section is in tension. Figure 8(c) suggests that the inverted T-beam system with tapered webs features the narrowest cast-in-place topping top of precast web interface and therefore minimizes the extent of potential longitudinal and transverse cracking.
Figure 9 shows the magnitude and distribution of longitudinal and transverse normal stresses along the depth of the three composite bridge cross-sections investigated. This distribution was obtained from the finite element models created for each bridge system. Transverse and longitudinal stress values were obtained from a column of finite elements located at mid-width of the composite cross-sections. Figure 9(a) shows that the magnitude of transverse normal stresses caused by time dependent effects in the three investigated bridge systems is similar. The voided slab system appears to be experiencing slightly smaller tensile stresses at the top of the cast-in-place topping due to the slightly more flexible restraint provided by the precast component as a result of the holes. However, this reduction is small compared to the advantage of a shorter critical interface offered by the inverted T-beam systems.

Figure 9(b) shows that the magnitude of longitudinal normal tensile stresses in the CIP topping is smaller in the precast inverted T-beam systems with tapered webs compared to the other two systems. The combination of smaller tensile stresses in the CIP topping and a shorter interface at the top of the precast web reduces not only the likelihood of transverse cracking but also the extent of it. Table 9 shows a comparison of the vulnerability to cracking of the three bridge systems in terms of the ratio between the maximum tensile stress at the bottom of the cast-in-place concrete deck and the tensile strength of the deck. The tensile strength of the concrete deck was taken equal to the tensile strength of the concrete mix with normal weight coarse aggregates and a portion of saturated lightweight fine aggregates. Table 9 shows that the bridge system with precast inverted T-beams features the lowest average ratio between the maximum tensile stress at the bottom of the deck and the tensile strength of the deck. Tapering the precast webs helps reduce the extent of the critical interface between the top of the precast web and the cast-in-place deck in both the transverse and longitudinal directions. Any tensile stresses developed at the interface between the precast flange and cast-in-place topping, or those created between the tapered precast webs and cast-in-place topping are less likely to cause cracking in the top surface of the bridge deck.

The selection of the inverted T-beam system with tapered webs for short-to-medium-span bridges combined with the specification of a cast-in-place concrete topping mix that exhibits low shrinkage and high creep will offer a bridge system that accelerates construction and is less likely to exhibit cracking due to time dependent effects.

CONCLUSIONS

Reducing the likelihood of bridge deck cracking is essential for increasing the longevity of bridges. This study has demonstrated that the effects of differential shrinkage and creep in composite bridges can cause tensile stresses in the deck that exceed its tensile strength. To reduce the likelihood of excessive cracking it is recommended that the concrete mix for the cast-in-place deck possesses low shrinkage and high creep properties. Low free shrinkage reduces the tensile stresses developed due to restrained differential shrinkage and high creep helps relax any tensile stresses that may develop. In addition, the short term properties that will help reduce the extent of cracking due to differential shrinkage include a mix with high tensile strength and low modulus of elasticity. Because it is difficult to find a concrete mix that embodies all the aforementioned long term and short term properties, priority should be given to a mix with the lowest shrinkage because it is the free shrinkage of the deck that serves as a catalyst for the creation of tensile stresses in the cast-in-place topping. In addition, sensitivity studies can be performed for a given structure to determine the influence of the short and long term properties of the concrete materials on the structural effects of shrinkage and creep. While a concrete mix with high creep is advocated for the cast-in-place deck to help alleviate tensile stresses due to differential shrinkage, long term deflections should be checked to ensure that they are within the allowable limits. Although the investigation described in this study was focused on slab-type short-to-medium-span composite concrete bridges, the benefits of a cast-in-place deck with low shrinkage and high creep apply also to composite girder-slab bridges in which the girder is either precast concrete or steel. In girder-slab bridges the free shrinkage of the deck is restrained by either the precast or steel girder. Such a restraint to the free shrinkage of the deck could lead to transverse and longitudinal cracks, which could affect the service life of the bridge.

Seven deck mixes developed by the researchers at VCTIR were investigated with the goal of identifying a mix with low shrinkage and high creep. Drying shrinkage strains recorded in the shrinkage prisms showed that the mix with normal weight coarse aggregates and saturated light weight fine aggregates exhibited the lowest shrinkage strain. In addition, data obtained from the creep test showed that the mix with normal weight coarse aggregates and saturated light weight fine aggregates also exhibited the highest creep coefficient. It should be noted that the tests performed on the deck mixes described in this investigation were performed only on one batch for each mix. It was outside the scope of study to investigate the repeatability and consistency of the results obtained from each mix.

Two methods for determining the structural effects of differential shrinkage and shrinkage induced creep were presented. The first is based on Menn's [1] approach and is suitable for a design office, because it can be easily implemented in a mathematical analysis program, such as Mathcad 14 [10], or in a computer spreadsheet program. The second method was based on finite element analysis and takes into account the 3D stress state and can be used in situations where such an analysis is an option. The results from both methods were compared for a slab-type composite concrete bridge and it was demonstrated that the first approach provided a reasonable estimation of the stresses due to time dependent effects for design purposes and is a viable alternative to finite element analysis.

Three composite bridge systems intended for short-to-medium-span bridges were investigated with the purpose of identifying the system that is most resistant against time dependent effects. The voided slab system is the traditional system and the inverted T-beam system with straight and tapered precast webs are relatively new bridge systems used in Minnesota and Virginia, respectively. The precast inverted T-beam system with tapered webs minimizes the width of the interface between the top of the precast web and the cast-in-place topping, which is the most vulnerable interface to longitudinal and transverse cracking as a result of differential shrinkage. While the magnitude of transverse normal stresses was similar in all three bridge systems, the inverted T-beam with the tapered webs exhibited lower longitudinal tensile stresses at the interface between the precast web and cast-in-place topping, which is desirable for reducing the likelihood of transverse cracking.

The results presented in this investigation suggest that the combination of the precast inverted T-beam system with tapered webs and the implementation of a cast-in-place topping mix with normal weight coarse aggregates and saturated light weight fine aggregates should help increase the resistance of short-to-medium-span bridges against time dependent effects.

NOTATION

A_D = area of cast-in-place deck
A_G = area of precast girder
A_{ps} = area of prestressing strands
a = distance between the centroid of cast-in-place deck and centroid of precast girder.
a_D = distance between the centroid of the cast-in-place deck and centroid of composite section
a_G = distance between the centroid of the girder and centroid of the composite section
E_D = modulus of elasticity of the cast-in-place deck
E_G = modulus of elasticity of the precast girder
E_{ps} = modulus of elasticity of prestressing strands
e = eccentricity of the prestressing force with respect to the centroid of the precast girder
f'_c = specified compressive strength of concrete for use in design, ksi (MPa)
I_D = moment of inertia of the cast-in-place deck
I_G = moment of inertia of the precast girder
K_1 = correction factor for source of aggregate
M_D^0 = initial moment in the deck due to forces applied to the composite system
$M_{Ddirect}^0$ =initial moment applied directly to the deck
M_G^0 =initial moment in the girder due to forces applied to the composite system
$M_{Gdirect}^0$ =initial moment applied directly to the girder
N_D^0 = initial axial force in the deck due to forces applied to the composite system
$N_{Ddirect}^0$ =initial axial force applied directly to the deck
N_G^0 =initial axial force in girder due to forces applied to the composite system
$N_{Gdirect}^0$ =initial axial force applied directly to the girder
N_{ps}^0 = initial prestressing force in the strand due to forces applied to the composite system
$N_{psdirect}^0$ = initial prestressing force in the strand
$\Delta\varepsilon_D$ = change in strain at the centroid of deck due to time dependent effects
$\Delta\varepsilon_G$ = change in strain at the centroid of girder due to time dependent effects
$\Delta\varepsilon_{ps}$ = change in strain in the prestressing strand due to time dependent effects
ΔX = change in curvature due to time dependent effects
ΔN_D = change in axial force in the deck due to time dependent effects
ΔN_G = change in axial force in the girder due to time dependent effects
ΔN_{ps} = change in prestressing force due to time dependent effects
ΔM_D = change in moment in the deck due to time dependent effects
ΔM_G = change in moment in the girder due to time dependent effects
w_c = unit weight of concrete, kcf (kg/m^3)

REFERENCES

[1] Menn, C.,1990, *Prestressed Concrete Bridges*, translated and edited by Paul Gauvreau, Birkhauser Verlag, Basel-Boston-Berlin, pp. 161-167.

[2] Darwin D., Browning J., *Project Summary: Phase I pooled fund study for the construction of crack-free concrete bridge decks*, The University of Kansas, http://www.iri.ku.edu/projects/concrete/bridgecrack.html (accessed January 2012)

[3] Ghali, A., Favre, R., Elbadry, M., 2012, *Concrete structures – Stresses and deformations: analysis and design for serviceability*, Spon Press.

[4] AASHTO, 2013, *LRFD Bridge Design Specifications*, 6th Edition, Washington, DC.

[5] ACI Committee 209.1R, 2005, *Report on Factors Affecting Shrinkage and Creep of Hardened Concrete* (ACI 209.1R-05), American Concrete Institute, Farmington Hills, MI.

[6] ACI Committee 209.2R, 2008, *Guide for modeling and calculating shrinkage and creep in hardened concrete* (ACI 209.2R-08), American Concrete Institute, Farmington Hills, MI.

[7] Partov, D., Kantchev, V., 2009, "Time-dependent analysis of composite steel-concrete beams using integral equation of volterra, according EUROCODE-4." *Engineering Mechanics* 16.5: 367-392.

[8] Bazant, Z.P., 1972, “Prediction of concrete creep effects using the age adjusted effective modulus method”, *ACI Journal,* V.69, No.4, pp. 212-217.

[9] Dilger, H.W., ”Creep analysis of prestressed concrete structures using creep transformed section properties”, *PCI Journal,* V.27, No.1, January-February 1982, pp. 98-117.

[10] Mathcad 14 User’s guide, (2007), Mathsoft Inc., Cambridge, Massachusetts.

[11] Barker, M., R., Puckett, A., J., 2007, *Design of highway bridges-an LRFD approach*, Second Edition, John Wiley & Sons, Inc.

[12] ASTM C39, 2010, *Test method for compressive strength of cylindrical concrete specimens*, American Society for Testing Materials, West Conshohocken, PA.

[13] ASTM C496, 2010, *Standard test method for splitting tensile strength of cylindrical concrete specimens*, American Society of Testing Materials, West Conshohocken, PA.

[14] ASTM C469, 2010, *Standard test method for static modulus of elasticity and Poisson’s ratio of concrete in compression*, American Society of Testing Materials, West Conshohocken, PA.

[15] ASTM C157, 2010, *Standard test method for length change of hardened hydraulic-cement mortar and concrete*, American Society of Testing Materials, West Conshohocken, PA.

[16] ASTM C512, 2010, *Standard test method for creep of concrete in compression*, American Society of Testing Materials, West Conshohocken, PA.

[17] Bazant, Z.P., 1987, “Statistical extrapolation of shrinkage data – Part I: Regression,” *ACI Materials Journal*, V.84, No.1, Jan.-Feb., pp 20-34.

Table 1 - Design Mixture Proportions for Topping Concrete

Mixture Proportions				
Constituent	NWC-FA lbs/yd^3 (kg/m^3)	NWC-SL1 lbs/yd^3 (kg/m^3)	SLWC-FA lbs/yd^3 (kg/m^3)	SLWC-SL lbs/yd^3 (kg/m^3)
Portland Cement	476 (283)	413 (245)	476 (283)	413 (245)
Fly Ash	159 (94)	0	159 (94)	0
Slag Cement	0	222 (132)	0	222 (132)
Water	286 (170)	286 (170)	273 (162)	273 (162)
Coarse Aggregate	1780 (1060)	1780 (1060)	901 (535)	901 (535)
NW Fine Aggregate	1030 (611)	1080 (641)	1360 (807)	1400 (831)
Total	3740 (2220)	3780 (2240)	3170 (1880)	3210 (1900)
Unit Weight	138 (82)	140 (83)	117 (70)	119 (71)
w/cm	0.45	0.45	0.43	0.43
Mixture Proportions (continued)				
Constituent	NWC-SLFA-SL lbs/yd^3 (kg/m^3)	NWC-SL2 lbs/yd^3 (kg/m^3)	NWC-SLFA lbs/yd^3 (kg/m^3)	
Portland Cement	382 (227)	382 (227)	635 (377)	
Fly Ash	0	0	0	
Slag Cement	254 (151)	254 (151)	0	
Water	261 (155)	286 (170)	261 (155)	
Coarse Aggregate	1730 (1030)	1730 (1030)	1730 (1030)	
NW Fine Aggregate	666 (395)	1290 (765)	666 (395)	
LW Fine Aggregate	403 (239)	0	403 (239)	
Total	3700 (2200)	3940 (2340)	3700 (2200)	
Unit Weight	137 (81)	146 (87)	137 (81)	
w/cm	0.41	0.45	0.41	

NWC-SL = normal weight coarse aggregate slag mix 1, NWC-FA = normal weight coarse aggregate fly ash mix, SLWC-SL = saturated light-weight coarse aggregate slag mix, SLWC-FA = saturated light-weight coarse aggregate fly ash mix, NWC-SLFA-SL = normal weight coarse aggregate with saturated light weight fines aggregates and slag, NWC-SL2 = normal weight coarse aggregate slag mix 2, NWC-SLFA = normal weight coarse aggregate with saturated light weight fines aggregates

Table 2 - Compressive strength test results

Age (days)	Compressive Strength, psi (MPa)						
	NWC-FA	NWC-SL1	SLWC-FA	SLWC-SL	NWC-SLWF-SL	NWC-SL2	NWC-SLWF
7	3100 (21)	3580 (25)	2600 (18)	4020 (28)	3660 (25)	4080 (28)	2650 (18)
14	3530 (24)	nm	3790 (26)	5270 (36)	4130 (29)	4830 (33)	3280 (23)
28	4260 (29)	5200 (36)	4600 (32)	5950 (41)	4560 (31)	5370 (37)	3540 (24)
56	4140 (29)	5250 (36)	4910 (34)	6420 (44)	nm	5410 (37)	3610 (25)
90	4060 (28)	5410 (37)	4880 (34)	6440 (44)	nm	nm	nm

nm=not measured, nc=not calculated

Table 3 - Tensile strength test results

Age (days)	Tensile Strength, psi (MPa)					
	NWC-FA			NWC-SL1		
	Tested	$Eqn.5.1$	Tested/($Eqn.5.1$)	Tested	$Eqn.5.1$	Tested/($Eqn.5.1$)
7	317 (2.2)	405 (2.8)	0.78	391 (2.7)	435 (3.0)	0.90
28	418 (2.9)	475 (3.3)	0.88	455 (3.1)	524 (3.6)	0.87
90	412 (2.8)	463 (3.2)	0.89	541 (3.7)	535 (3.7)	1.01
			Avg. = 0.85			Avg. = 0.93
	SLWC-FA			SLWC-SL		
	Tested	$Eqn.6.1$	Tested/($Eqn.6.1$)	Tested	$Eqn.6.1$	Tested/($Eqn.6.1$)
7	274 (1.9)	322 (2.2)	0.85	374 (2.6)	401 (2.8)	0.93
28	370 (2.6)	429 (3.0)	0.86	391 (2.7)	488 (3.4)	0.80
90	435 (3.0)	442 (3.1)	0.98	503 (3.5)	508 (3.5)	0.99
			Avg. = 0.90			Avg. = 0.91
	NWC-SLWF-SL			NWC-SL2		
	Tested	$Eqn.5.1$	Tested/($Eqn.5.1$)	Tested	$Eqn.5.1$	Tested/($Eqn.5.1$)
7	377 (2.6)	440 (3.0)	0.86	417 (2.9)	470 (3.2)	0.89
28	370 (2.6)	470 (3.2)	0.79	483 (3.3)	510 (3.5)	0.95
90	nm	nc	nc	nm	nc	nc
			Avg. =0.83			Avg. = 0.92
	NWC-SLWF			Summary of Tested Values (28 days) f_t, psi (MPa)		
	Tested	$Eqn.5.1$	Tested/($Eqn.5.1$)	NWC-FA		418 (2.9)
7	287 (2.0)	370 (2.6)	0.78	NWC-SL1		455 (3.1)
28	340 (2.3)	420 (2.9)	0.81	SLWC-FA		370 (2.6)
90	nm	nc	nc	SLWC-SL		391 (2.7)
			Avg. = 0.80	NWC-SLWF-SL		370 (2.6)
				NWC-SL2		483 (3.3)
				NWC-SLWF		340 (2.3)

nm=not measured, nc=not calculated

Table 4 - Modulus of elasticity test results

Age (days)	Modulus of Elasticity, ksi (Mpa)					
	NWC-FA			NWC-SL1		
	Tested	$Eqn.7.1$	Tested/ $Eqn.7.1$	Tested	$Eqn.7.1$	Tested/$Eqn.7.1$
7	4530 (31200)	3220 (22200)	1.41	4760 (32800)	3350 (23100)	1.42
14	4280 (29500)	3430 (23700)	1.25	nm	nc	nc
28	4430 (30600)	3770 (26000)	1.18	5010 (34500)	4040 (27900)	1.24
56	4150 (28600)	3720 (25700)	1.12	5180 (35700)	4060 (28000)	1.28
90	4360 (30100)	3680 (25400)	1.18	4730 (32600)	4120 (28400)	1.15
			Avg. = 1.23			Avg. = 1.27
	SLWC-FA			SLWC-SL		
	Tested	$Eqn.7.1$	Tested/ $Eqn.7.1$	Tested	$Eqn.7.1$	Tested/$Eqn.7.1$
7	2620 (18100)	2230 (15400)	1.17	2780 (19200)	2690 (18600)	1.03
14	3180 (21900)	2680 (18500)	1.19	3160 (21800)	3080 (21200)	1.03
28	3080 (21200)	2970 (20500)	1.04	3540 (24400)	3270 (22600)	1.08
56	3460 (23900)	3070 (21200)	1.13	3260 (22500)	3390 (23400)	0.96
90	2950 (20300)	3060 (21100)	0.96	3010 (20800)	3400 (23400)	0.89
			Avg. = 1.10			Avg. = 1.00
	NWC-SLWF-SL			NWC-SL2		
	Tested	$Eqn.7.1$	Tested/ $Eqn.7.1$	Tested	$Eqn.7.1$	Tested/$Eqn.7.1$
7	3700 (25500)	3200 (22100)	1.16	4840 (33400)	3720 (25700)	1.30
14	3390 (23400)	3400 (23400)	1.00	4960 (34200)	4050 (27900)	1.23
28	4160 (28700)	3570 (24600)	1.17	5460 (37700)	4270 (29400)	1.28
56	nm			4950 (34100)	4280 (29500)	1.16
90	nm			nm		
			Avg. = 1.11			Avg. = 1.24
	NWC-SLWF			Summary of Tested Values, E (28 days), ksi (MPa)		
	Tested	$Eqn.7.1$	Tested/ $Eqn.7.1$	NWC-FA		4430 (30600)
7	3510 (24200)	2720 (18800)	1.29	NWC-SL1		5010 (34500)
14	4295 (29600)	3030 (20900)	1.42	SLWC-FA		3080 (21200)
28	3990 (27500)	3150 (21700)	1.27	SLWC-SL		3540 (24400)
56	4670 (32200)	3180 (21900)	1.47	NWC-SLWF-SL		4160 (28700)
90	nm			NWC-SL2		5460 (37700)
			Avg. = 1.36	NWC-SLWF		3990 (27500)

nm = not measured, nc = not calculated

Table 5 - Summary of experimental shrinkage strains at 100 days

Mix	Shrinkage strains at 100 days (ue)
NWC-FA	466
NWC-SL1	483
SLWC-FA	603
SLWC-SL	606
NWC-SLWF-SL	310
NWC-SL2	264
NWC-SLWF	215

Table 6 - Summary of experimental data from the creep tests

	NWC-FA	NWC-SL1	SLWC-FA	SLWC-SL	NWC-SLWF-SL	NWC-SL2	NWC-SLWF
Elastic strain (ue)	439	442	711	720	470	498	372
Shrinkage strain (ue)	402	358	527	321	276	214	260
Creep strain (ue)	819	548	868	502	416	511	719
Total strain (ue)	1660	1348	2106	1543	1162	1223	1351
Creep Coefficient	1.87	1.24	1.22	0.70	0.89	1.03	1.93

Table 7 - Summary of experimental data on shrinkage and creep properties (100 days)

Mix	Drying shrinkage strain (ue)	Creep coefficient
NWC-FA	466	1.87
NWC-SL1	483	1.24
SLWC-FA	603	1.22
SLWC-SL	606	0.70
NWC-SLWF-SL	310	0.89
NWC-SL2	264	1.03
NWC-SLWF	215	1.93

Table 8 - Comparison of tensile stresses in the deck and the tensile strength of the deck

Mix	f_{tmax}, ksi (MPa)	$f_{ttested}$, ksi (MPa)	Ratio = $f_{tmax}/f_{ttested}$
NWC-FA	0.504 (3.5)	0.418 (2.9)	1.21
NWC-SL1	0.653 (4.5)	0.455 (3.1)	1.44
SLWC-FA	0.591 (4.1)	0.370 (2.6)	1.60
SLWC-SL	0.756 (5.2)	0.390 (2.7)	1.94
NWC-SLWF-SL	0.407 (2.8)	0.370 (2.6)	1.10
NWC-SL2	0.399 (2.8)	0.483 (3.3)	0.83
NWC-SLWF	0.214 (1.5)	0.340 (2.3)	0.63

Table 9 - Comparison of the vulnerability to cracking of the three bridge systems

Bridge system	Direction of stress	f_{tmax}, ksi (Mpa)	$f_{ttested}$, ksi (Mpa)	Ratio = $f_{tmax}/f_{ttested}$	
Voided Slab	S11	0.240 (1.7)	0.340 (2.3)	0.71	Average = 0.70
	S33	0.236 (1.6)	0.340 (2.3)	0.69	
Precast inverted T-beam with straight webs	S11	0.250 (1.7)	0.340 (2.3)	0.74	Average = 0.68
	S33	0.210 (1.5)	0.340 (2.3)	0.62	
Precast inverted T-beam with tapered webs	S11	0.255 (1.8)	0.340 (2.3)	0.75	Average = 0.61
	S33	0.156 (1.1)	0.340 (2.3)	0.46	

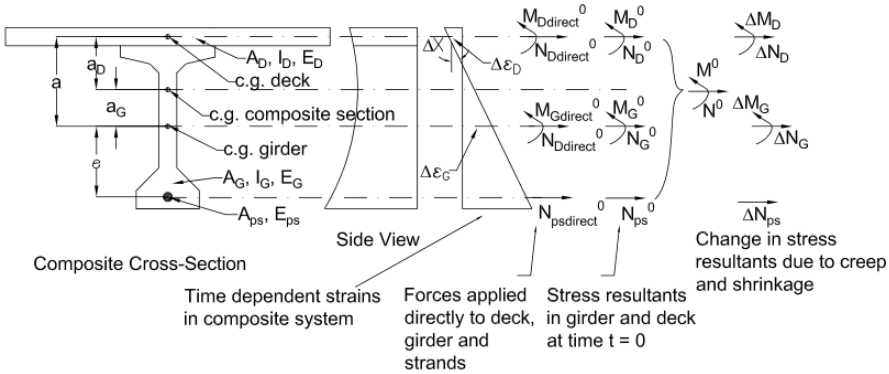

Fig. 1- Redistribution of forces in composite girders

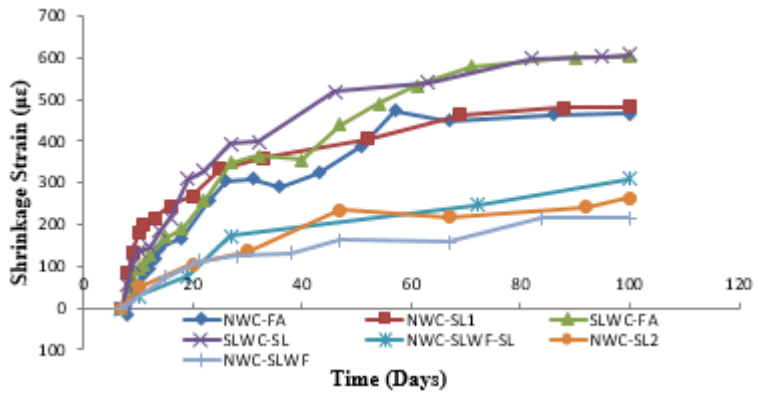

Fig. 2 - Experimental data on shrinkage strain versus time (unrestrained shrinkage test)

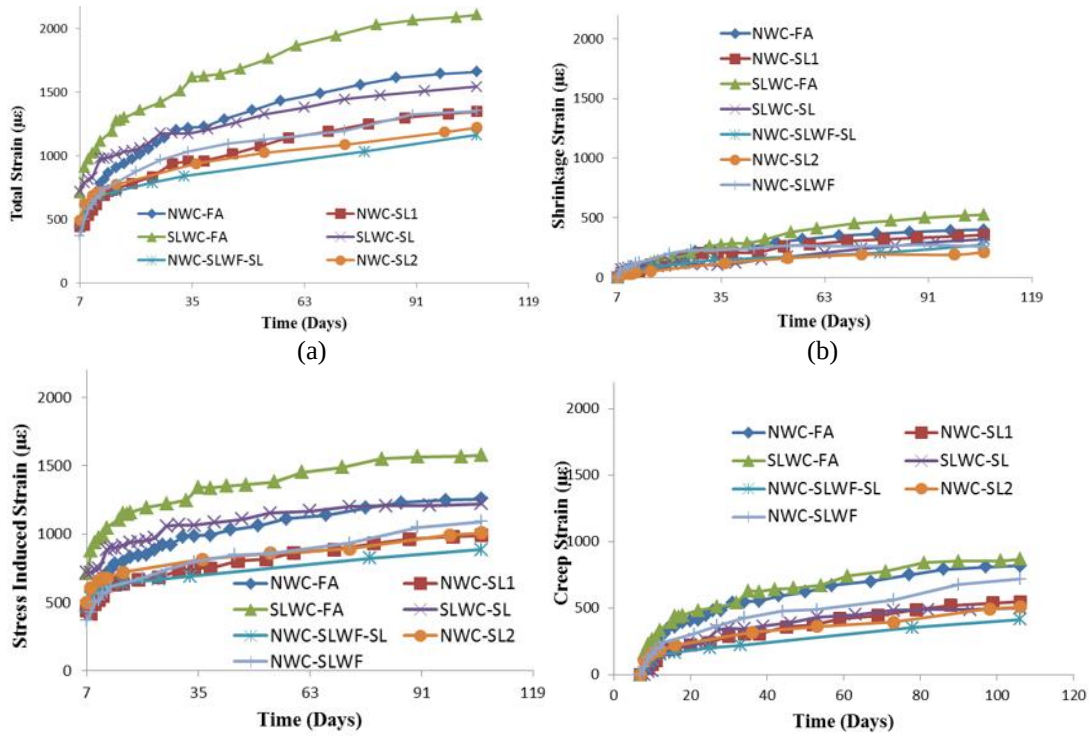

Fig. 3 - Creep test – (a) total strain, (b) shrinkage strain, (c) stress induced strain, (d) creep strain

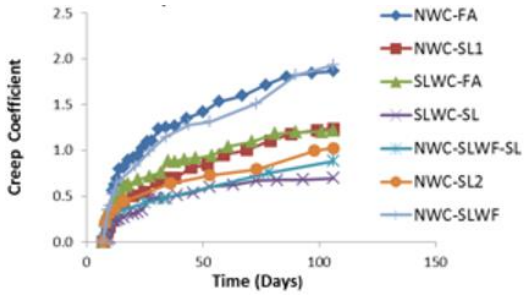

Fig. 4 - Creep coefficient vs time

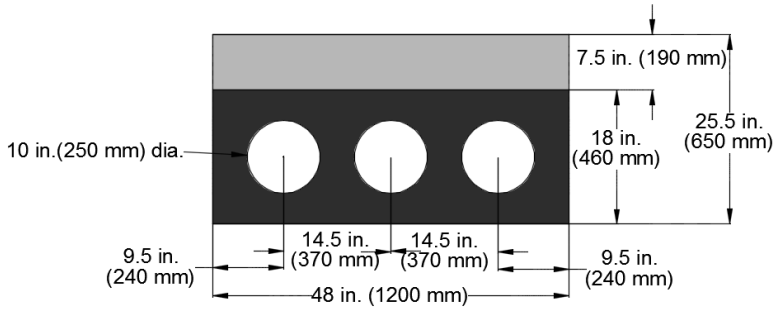

Fig. 5 - Cross-section of composite voided slab system

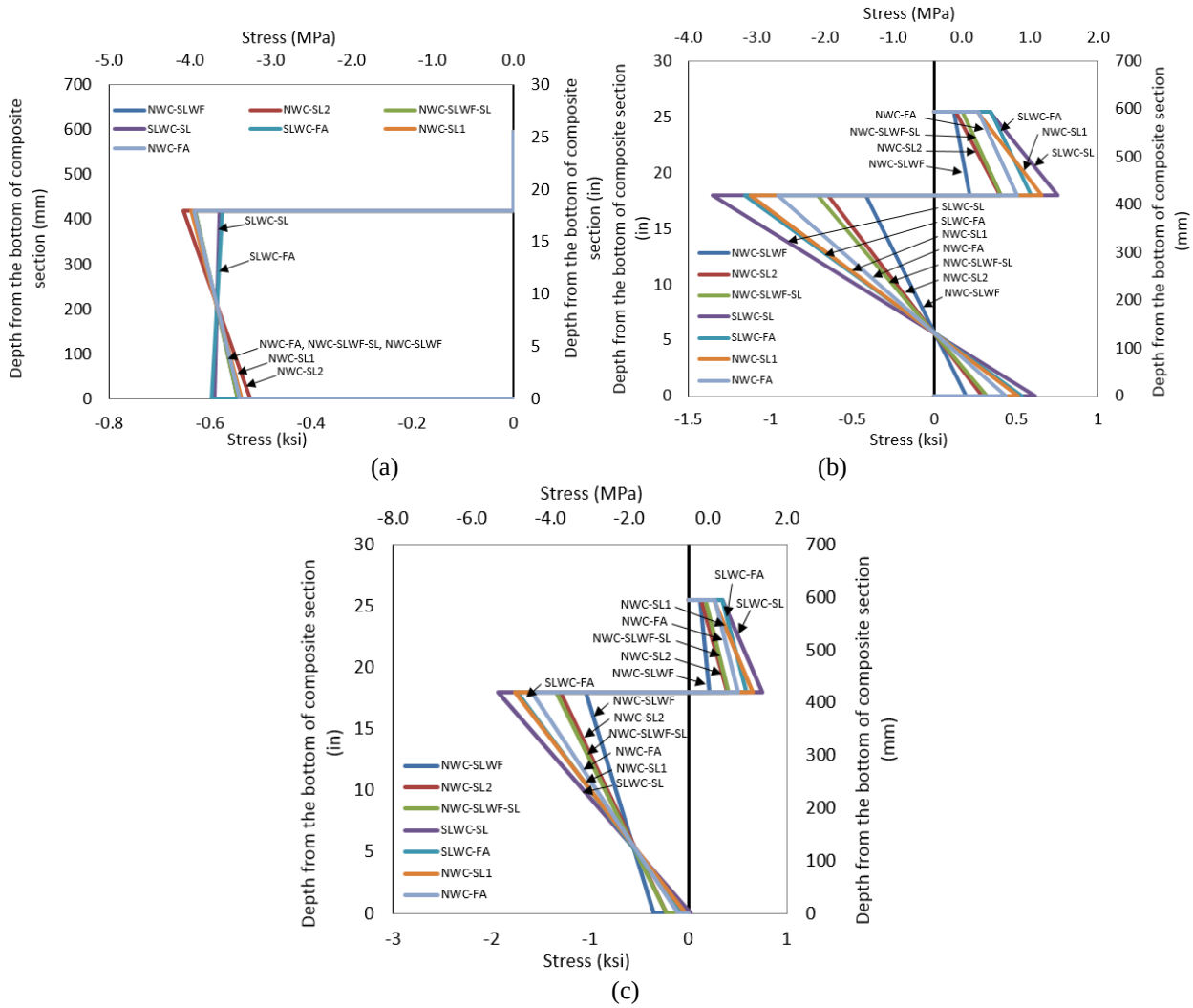

Fig. 6 - Stresses in composite voided slab system (a) initial stresses due to mechanical loads, (b) changes due to time dependent effects, (c) final stresses

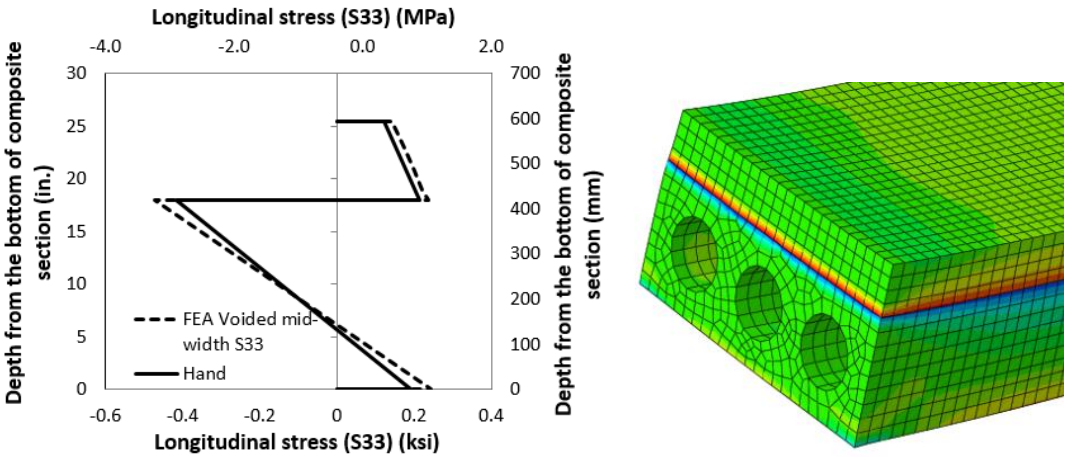

(a) (b)

Fig. 7 - (a) Distribution of longitudinal normal stresses in the composite voided slab system due to differential shrinkage and shrinkage induced creep (b) Longitudinal normal stress contours in the composite voided slab system

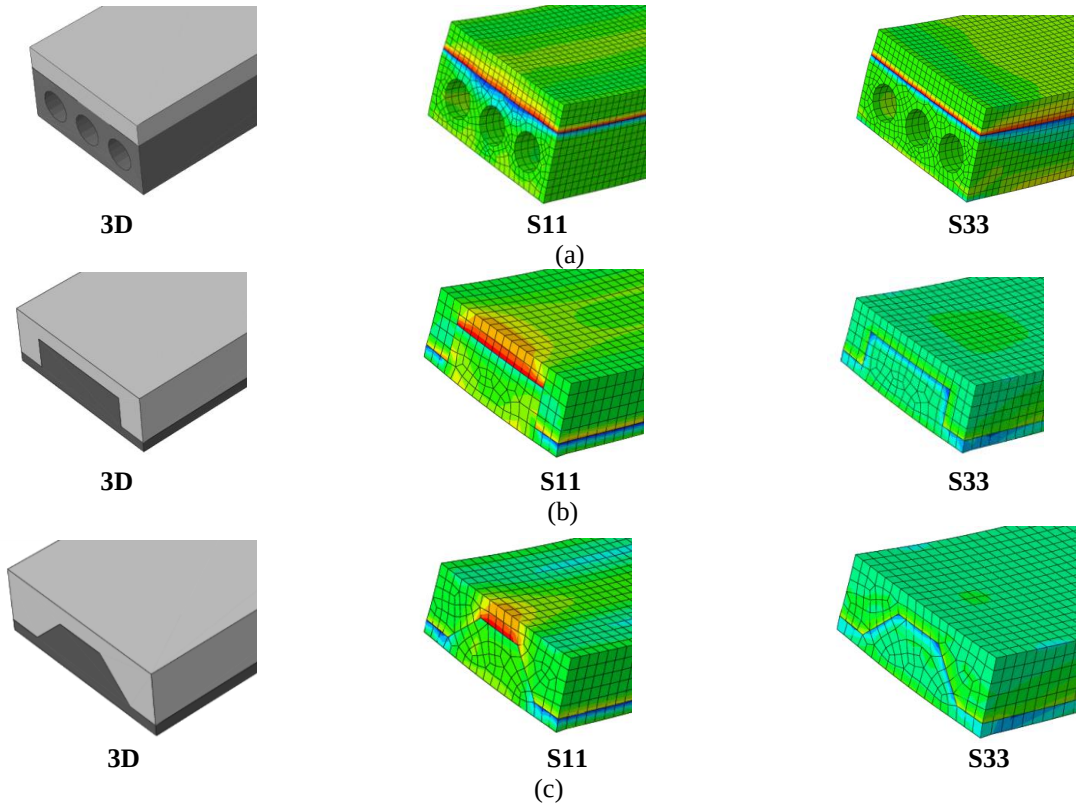

Fig. 8 - Transverse (S11) and longitudinal (S33) normal stresses for three composite bridge systems due to differential shrinkage and shrinkage induced creep

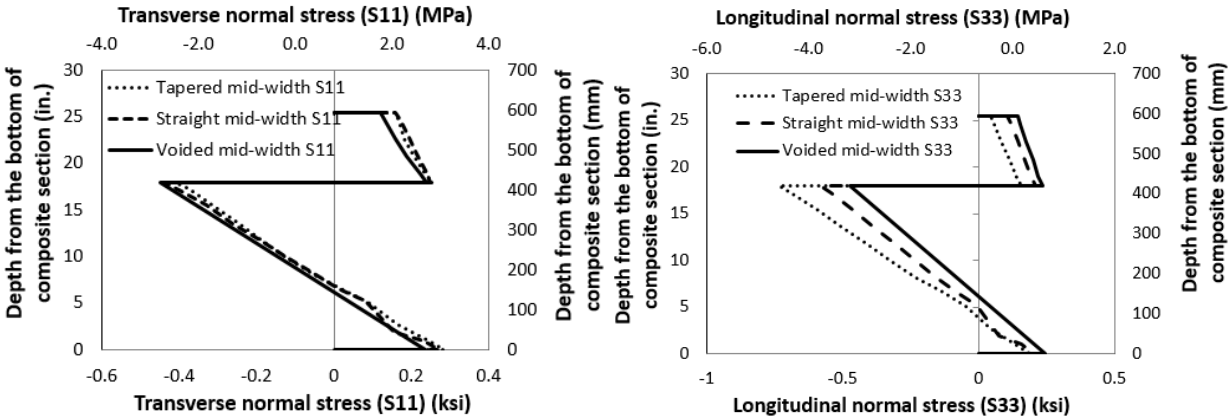

(a) (b)

Fig. 9 - Comparison of normal stresses in three composite bridge systems caused by differential shrinkage and shrinkage induced creep, (a) Transverse normal stresses, (b) Longitudinal normal stresses